UNIVERSIDAD DE CONCEPCIÓN
FACULTAD DE CIENCIAS FÍSICAS Y MATEMÁTICAS

CHARACTERIZATION OF HISTORICAL MEGATHRUST EARTHQUAKE RUPTURES IN SOUTH CENTRAL CHILE USING LOGIC TREE ANALYSIS

Por Javiera San Martín Parra

Tesis presentada a la Facultad de Ciencias Físicas y Matemáticas para optar al grado de Magíster en Geofísica.

Profesora Guía: Dra. Ignacia Calisto Burgos
Comisión: Dra. Lisa Ely,
Dr. Marcos Moreno,
Dr. Jorge Quezada

Abril 2023
Concepción, Chile

UNIVERSIDAD DE CONCEPCIÓN
FACULTAD DE CIENCIAS FÍSICAS Y MATEMÁTICAS

CHARACTERIZATION OF HISTORICAL MEGATHRUST EARTHQUAKE RUPTURES IN SOUTH CENTRAL CHILE USING LOGIC TREE ANALYSIS

Javiera San Martín Parra

Tesis presentada a la Facultad de Ciencias Físicas y Matemáticas de la Universidad de Concepción para optar al grado de Magíster en Geofísica.

Profesora Guía: Dra. Ignacia Calisto
Comisión: Dra. Lisa Ely,
Dr. Marcos Moreno,
Dr. Jorge Quezada

Abril 2023, Concepción, Chile.

Dedicado a mi Madre

AGRADECIMIENTOS

Quiero expresar mi más sincero agradecimiento a todas las personas que hicieron posible la realización de esta tesis.

En especial a mi familia y amigos, quienes siempre tuvieron las palabras indicadas para hacer que este camino fuera más llevadero. Sin su compañía, este trabajo jamás habría sido posible.

Quiero agradecer a todo el equipo de trabajo, en especial a Ignacia, por guiarme a lo largo de todo el proceso de investigación, siempre con una palabra de motivación y empatía. A mis compañeros, especialmente a Rodrigo, por su infinita paciencia y colaboración en cada una de las dudas que surgían en el camino.

El presente estudio está financiado por el proyecto FONDECYT 11180854 "Caracterización de fuentes para tsunamis históricos en el centro-sur de Chile", dirigido por Ignacia Calisto, PhD. Se brindó apoyo y financiamiento adicional a través de la Iniciativa Científica Milenio (ICM) con el número de subvención NC160025 "Núcleo Milenio CYCLO: El Ciclo Sísmico a lo largo de Zonas de Subducción".

Abstract

Characterizing the spatial distribution of ruptures from historical and recent earthquakes is key to understanding the seismic cycle of large earthquakes in subduction zones, and thus to assessing the potential risks associated with future earthquakes. The southern portion of Central Chile (35°S-38°S) has been continuously affected by large earthquakes, such as the 2010 Maule (Mw 8.8) and the 1835 earthquakes witnessed by Robert Fitzroy (HMS Beagle captain). Our goal is to identify the rupture pattern and tsunami propagation of the 1570, 1657, 1751, 1835, and 2010 mega-earthquakes, events that overlapped in central Chile, by compiling historical records and applying robust statistical tools. We used an adaptation of a logic tree methodology to generate random sources of slip distribution for each event, constrained by tsunami and deformation data. We find that the three events studied have different slip peaks. The 1751 earthquake has the largest slip with a maximum patch of $\sim$ 26 m, while the 2010 and 1835 earthquakes reach slips of $\sim$ 16 m and $\sim$ 10 m, respectively. Our results show that a part of the segment between 36°S and 37°S was consistently affected by large earthquakes, but with different slip and depth. The northern part of the segment accumulated energy for at least 300 years and was released by the 2010 earthquake. This work provides important information for identifying rupture patterns between historical and recent earthquakes, and highlights the importance of extending the time scale of earthquake slip distribution analyses to multiple cycles to describe both earthquake characteristics and their spatial relationship, and thus gain a better understanding of seismic hazard.

Contents

List of Tables

List of Figures

Chapter 1

Introduction

1.1 South Central Chile Segment

The southern portion of the Central segment corresponds to a delimited area extending from approximately 35° to 38°S; representing a portion of the Chilean subduction zone, where megathrust earthquakes occur (Bilek and Lay, 2018). The most recent event is the Mw 8.8 Maule earthquake on February 27, 2010, for which proposed rupture lengths range from 500 to 600 km (Delouis et al. 2010; Lay et al. 2010; Lorito et al. 2011; Lay et al. 2012; Moreno et al. 2012; Metois et al. 2012). This event closed a seismic gap initiated by the 1835 earthquake, which ruptured the southern part of this segment (Vigny et al. 2011). In the last 400 years, at least 5 earthquakes M $\geq$ 8 have been recorded in the South Central segment, these events corresponds to the years 1570, 1657, 1751, 1835, and 2010 (Fig. 1.1.1), indicating that here, a megathrust earthquake occurs in average every 110 years, which is a frequent seismic activity rate for this type of earthquake. Earthquakes of M $<$ 8 have also been recorded in the northern part of the segment in 1928, 1939 and 1953 (Beck et al. 1998).

Characterization of these events has been made through different methods and disciplines, such as paleoseismology of tsunamis. In the South Central segment, paleotsunami deposits have been found in the southern portion of the segment, near Quidico and rua. (Ely et al. 2014; Dura et al. 2015; Dura et al. 2017; Hong et al. 2017). Historical records and geological observations have also contributed to the inference of earthquake magnitude and extent, such as tsunami propagation and

wave height (Fitz Roy, 1839; Darwin, 1860; Soloviev and Go, 1975; Lomnitz, 2004; Quezada et al. 2012; Stewart, 2019). Uncertainties in categorical or numerical information for historical tsunami earthquakes significantly affects results. We follow the methodology proposed by Cifuentes et al. (2023) that uses a logic tree approach to generate multiple and random scenarios. This method computes random fault source models, compares them to observations, and then refines the models to better match those observations.

Then, it is possible to identify the most likely slip distribution model of a megathrust earthquake, taking into account the uncertainties involved. Our goal is to characterize and compare the 1751, 1835, and 2010 events. Identifying areas of large energy release and asperities can provide insights into the frequency and location of earthquakes within specific segments. The selection of these earthquakes was according to the magnitude M $\geq$ 8, tsunami effects, and availability of data for deformation and tsunami wave height.

The characterization of earthquakes along a segment is an essential task for the development of hazard-resilient communities in terms of seismic events, since it allows to approximate recurrence intervals in a delimited area (Nishenko et al. 1991; Philibosian et al. 2020) as well as the earthquake effects. Relying solely on recent or well-documented events for hazard studies may lead to an underestimation of the potential impact of future earthquakes. As the energy released by earthquakes is not uniformly distributed along-strike and along-dip, the contribution of each event is crucial for identifying activity in different parts of the segment (Lay et al. 2012). To achieve a comprehensive assessment of seismic hazard, it is important to consider long-scale temporal records, as highlighted by Dura et al. (2014). Therefore, including a wide range of earthquake data, both recent and historical, is essential for accurately assessing seismic risk and developing effective disaster mitigation strategies.

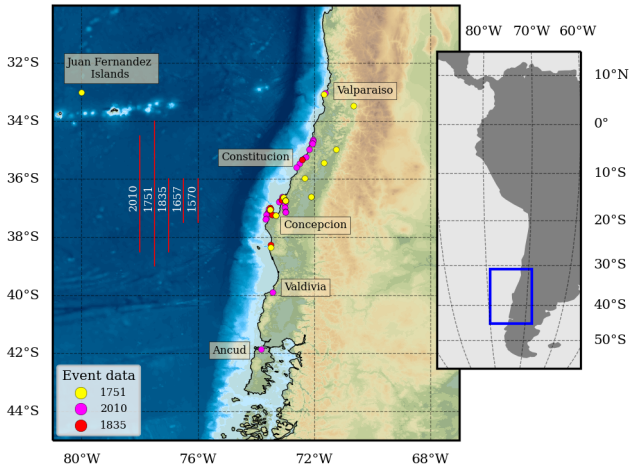

Figure 1.1.1: The referential map (right) highlights the study region in a blue rectangle. The zoom-in (left) shows the spatial distribution of data availability per event in the study area (deformation and tsunami data); yellow, magenta, and red dots represents data for 1751, 2010, 1835 events, respectively. Vertical red lines indicates the approximate latitudinal extent of 1570, 1657, 1751, 1835, and 2010 ruptures.

1.2 Generation

The seismic cycle in subduction zones is a period of time that can last from decades to hundreds of years (Ruiz et al. 2018), where there is an accumulation of energy commonly caused by a locking at the interface of tectonic plates, which in turn depends on structural and frictional factors. This locking is known as plate coupling (Vigny et al. 2009; Moreno et al. 2010) and controls the characteristics of the deformation field in the area, causing uplift or subsidence movements on the coast, which occur mainly when there is an abrupt release of energy during an earthquake.

The seismic cycle is described by the different stages that compose it (see Table 1.2.1) and the changes in the tectonic configuration or deformation field where the earthquake occurs.

The great variability of earthquakes denote a hallmark of each seismic cycle; depending not only on geometric factors (such as the depth and size of the event) but also on the structural and frictional control of the zone in which they occur (Shi et al., 2020). In addition, the rupture length of an earthquake determines an important factor in variability, depending on whether it ruptures the entire plate

interface in the segment or only generates a partial rupture of the segment (Ruiz et al., 2018).

Period	Description	Time
Interseismic	Pre-earthquake loading period corresponds to the accumulation of stresses at the plate interface as a result of plate locking or coupling and subduction of the oceanic plate beneath the continental plate.	Decades to hundreds of years.
Coseismic	Period in which the release of energy from the seismic event occurs.	Seconds to minutes.
Post seismic	This period is characterized by the gradual release of energy that was not released during the co-seismic.	Decades of years.

Table 1.2.1: Seismic cycle

When an earthquake occurs, the seafloor deforms greatly above the fault source. At the same time, seismic waves radiating from the fault source propagates horizontally and moves away from the fault region rapidly, while the seafloor displacement remains close to the fault region. Deformation of the seafloor displaces water, then the sea surface rises. As time passes, gravity causes the raised sea surface to collapse; the collapsed volume of water displaces a massive volume of water in the horizontal direction, and the displacement of the sea surface propagates as a long-length wave. This water wave is the tsunami. On the other hand, the propagation of seismic waves depends mainly on the elasticity of the medium (Saito, 2019).

1.3 Propagation

The shallow water equations describe a number of physical characteristics, including wave dynamics, in which alterations in sea surface height move as waves. The linear shallow water equation associated with tsunami generation by small bottom deformations, in a homogeneous ocean of constant depth H, without

taking into account surface and bottom stresses, Coriolis force and viscous terms can be expressed as (Eze, et al., 2009):

$$\frac{\partial U}{\partial t} + gH\frac{\partial \eta}{\partial x} = 0 \tag{1.3.1}$$

$$\frac{\partial V}{\partial t} + gH\frac{\partial \eta}{\partial y} = 0 \tag{1.3.2}$$

$$\frac{\partial \eta}{\partial t} + \left(\frac{\partial U}{\partial x} + \frac{\partial V}{\partial y}\right) = 0 \tag{1.3.3}$$

Where

- η : Vertical displacement of the water surface on an equipotential surface.
- t : Time elapsed.
- U, V: Horizontal and vertical component of the water surface.
- g : Gravity acceleration.

The combination of these equations gives us the expression:

$$\frac{\partial^2 \eta}{\partial t^2} - gH\nabla^2\eta = 0 \tag{1.3.4}$$

Deriving the expression for the one-dimensional case:

$$\frac{\partial^2 \eta}{\partial t^2} - gH\frac{\partial^2 \eta}{\partial x^2} = 0 \tag{1.3.5}$$

The above equation has the form of the wave equation, therefore, we can propose the following solution:

$$\eta = \exp i(kx - \omega t) \tag{1.3.6}$$

The equation 1.3.6 will be a solution if and only if:

$$\omega = \sqrt{gHk} \tag{1.3.7}$$

Where

- ω: Wave frequency
- k: Wave number

Using surface wave theory, the dispersion relation will be, in effect:

$$\omega^2 = gktanh(kH) \tag{1.3.8}$$

The relationship 1.3.8 shows that the waves generated by a tsunami must be considerably longer than the ocean depth for the consideration of shallow waves to be valid. In the case of the Pacific Ocean, the average depth is about 4 km; while tsunami wavelengths are about 300-400 km, so the above equations are valid (Fujima, et al., 2002).

1.4 Logic tree approach

The logic tree approach corresponds to a machine learning algorithm used to solve regression and classification problems. This technique is used to predict the value of a target variable by combining parameters. Annaka et al. 2007 used this methodology for the development of a probabilistic analysis of tsunami risk in the coasts of Japan, thus obtaining a long-term projection that allows knowing the associated risk, for example, through the recurrence periods of an event. In this work, an adaptation of such methodology is proposed, with the difference that it will not be used to project tsunami risks in the future but will be used to know the probable characteristics of the source of past earthquakes (and respective tsunamis), characterized through their magnitude, slip distribution and geographical limits. Figure 1.4.1 shows a scheme used to characterize the Concepción 1570 earthquake.

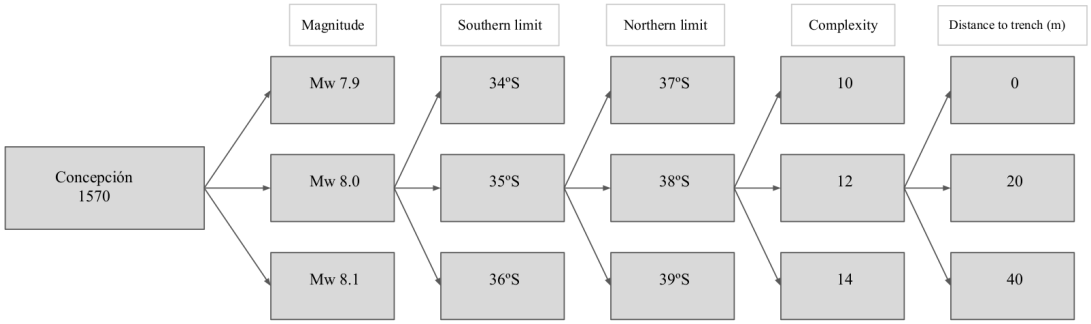

Figure 1.4.1: Example of logic tree branches for the characterization of the Concepción 1570 event.

As shown in 1.4.1, the tree is composed of nodes and branches. The nodes represent the different parameters to be used: earthquake magnitude, northern limit, southern limit, complexity and aspect ratio. The last two being a measure of the amount of slip variation between contiguous faults and the ratio between the large and width of the fault. The branches represent the alternatives of possible values that each node can take, therefore each branch is assigned a probability of occurrence. Once the different sources have been obtained, the models must be restricted and selected according to the constraints addressed in the next subsection. An example of these are the observations of tsunamis for events prior to the 20th century, which despite being scarce, can be found in historical records, e.g. the letters kept by the General Archive of the Indies, Spain, which describe through accounts some effects and consequences of earthquakes and tsunamis in the 18th century.

1.5 Goals and objectives

1.5.1 General objective

Characterize historical tsunami sources in Central Chile segment (34.0°S - 38.2°S), by using the logic tree approach, and historical constraining models from observations found in the literature (e.g. magnitude, epicenter, fault parameters: length, width, depth, slip) and paleotsunami stratigraphic records (e.g. deformation, wave height, inundation) and historical information.

1.5.2 Specific objectives

1. Bibliographic compilation from different historical events in the segment and creation of the logic tree branches.
2. Use the logic tree approach to characterize historical tsunamis and obtain the source models parameters associated with each event.
3. Simulate tsunamis generated by different source models for each historical earthquake to obtain tsunami heights and compare with tsunami heights observations.
4. Identify similarities or variations between events to determine possible

patterns in the seismic cycle.

1.6 Hypotheses

1. The most probable sources of historical tsunamis occurring in the Central Chile segment can be estimated with the logic tree approach which combines different source parameters (e.g. magnitude, length, width, slip and depth). The application of constraints from the theory of characteristic earthquakes (e.g. empirical relations) and observations from literature (e.g. crustal deformation, coastal uplift and subsidence, tsunami wave height and inundation) allow limiting the solutions to realistic or probable realizations of the model.

2. Quantification of the uncertainties in the solutions can be modeled with probabilistic analysis methods to give an idea of the range of possible tsunamis in the Central Chile subduction segment.

3. The models obtained allow an inter-event analysis to understand the determinants that control the seismic cycle in the same segment.

Chapter 2

Methodology

We follow the methodology presented in Cifuentes-Lobos et al. (2023), that computes heterogeneous slip distribution models and its deformation field, respectively, which are subjected to a set of constraints based on observations of vertical deformation, and wave height data. With the new subset of fault models, we perform a frequency analysis to obtain the most probable fault source. The result is a slip distribution that represents the most realistic scenario according to the availability of observational data. Given the different slip distributions for each event and the availability of observations to restrict it, it is possible to approximate the position of asperities along-dip and along-strike. Uncertainty is handled by statistical techniques such as maximized probability density function, and frequency analysis of the parameters used in the combination of the logic tree branches. To obtain the source models, we divided the methodology into two steps: 1) compilation of historical earthquake information and 2) logic tree parameter combination.

2.1 Generation of random tsunami sources

For the first part, random slip distribution are generated through a logic tree approach, where multiple combinations are made from giving a range of values to elemental earthquake parameters such as magnitude (Mw), latitudinal limits (in degrees) along-strike, distance to the trench imposes limitations on the allowable range of longitudes and depth (in particular case of Chilean subduction zone).

The aspect ratio of the fault and complexity did not correspond to a range of values, and it was a set as a single number. Fault width and length corresponds to geometrical parameters that set the aspect ratio of the fault. Every range of values is represented as a branch of the logic tree, thus chosen values play a key role in the model generation. Our definition of the range of parameter values varies depending on the earthquake and the available information for each. The criteria used to choose the values are subject to the availability of both categorical and numerical information. We consider in all cases the same number of values for parameters of complexity, distance to trench and aspect ratio, only differing in values of magnitude and geographical limits. Therefore, the ranges of the parameters, shown in Table 2.1.1, are narrower when more accurate information is available. A total of 8640 candidate models were computed for the 1570, 1657, and 2010 earthquakes by combining logic tree branches. Additionally, 25200 and 14400 candidate models were computed for the 1751 and 1835 earthquakes respectively using the same methodology.

For the restrictions mentioned earlier, we compare the models with observations of the amount and type of the deformation, whether uplift or subsidence, and tsunami wave height. Since 1570 and 1657 appear to have similar magnitudes (close to 8), and we presume both had rupture extent within Maule segment but possibly differing in northern and southern limits, we used the same parameter combination for both, saving the computational costs that would mean generating 2 combinations that differ slightly instead of generating 1 that covers a little more but can cover the characteristics of both.

To obtain the modeled tsunami wave, the vertical seafloor deformation field is calculated according to the Okada (1985) solution from each slip distribution model. The tsunami propagation is computed using COMCOTv1.7 (Cornell Multigrid Coupled Tsunami model, Wang, 2009).

Table 2.1.1: Logic tree earthquake parameters. Columns are designated according to year of the event, magnitude (Mw), northern limit and southern limit in degrees for each event.

Year	Magnitude (Mw)	Northern limit (°)	Southern limit (°)
1570	[7.8, 7.9, 8.0, 8.1, 8.2, 8.3]	[-34.0, -35.0, -36.0]	[-38.0, -39.0, -40.0]
1657	[7.8, 7.9, 8.0, 8.1, 8.2, 8.3]	[-34.0, -35.0, -36.0]	[-38.0, -39.0, -40.0]
1751	[8.6, 8.7, 8.8, 8.9, 9.0, 9.1]	[-33.0, -33.5, -34.0, -34.5, -35.0]	[-39.0, -39.5, -40.0, -40.5, -41.0]
1835	[8.3, 8.4, 8.5, 8.6, 8.7]	[-34.0, -35.0, -36.0]	[-37.0, -38.0, -39.0]
2010	[8.6, 8.7, 8.8, 8.9]	[-33.5, -34.0, -34.5]	[-37.5, -38.0, -38.5]

2.2 Model analysis

We perform the slip distribution analysis following the methodology of Cifuentes-Lobos et al. (2023). Once we obtain the number of models that comply with the imposed restrictions, we apply a frequency analysis to determine the mode of each parameter, and thus work with those that meet the values of the mode. The next step is to calculate the maximized probability density function (PDF) to obtain the most probable amount of slip in each subfault of the fault model, and thus the most probable position of the main slip patches. As this calculation may cause some irregularities in the distribution, we finally apply a Gaussian filter for smoothing the slip distribution model.

2.3 Historical information for data restrictions

The compilation of historical information provides observations and useful data to use as input in the deformation and tsunami wave height restrictions. Qualitative information is considered as categorical data that can indicate whether a location experienced uplift or subsidence deformation, or if a tsunami wave reached an area. Numerical data is also useful to constrain amounts of deformation or wave amplitude. Numerous efforts have been made to characterize past events, but many of them rely primarily on the qualitative description of damages and effects. The most widely utilized documents to accomplish this task can be found in the

"Archivo General de las Indias" (AGI), "Archivo Nacional de Chile" (e.g. Lomnitz, 1970; Lomnitz, 2004; Udias et al. 2012; Palacios, 2012) for characterizing the 1751 earthquake, and in Darwin (1860) and Fitz Roy (1839) for characterizing the 1835 earthquake. In the case of the 2010 earthquake, being a recent event, there are plenty of data describing its effects as well as numerical models representing the slip distribution (Lay et al. 2010; Delouis et al. 2010; Lorito et al. 2011; Vigny et al. 2011; Moreno et al. 2012).

2.3.1 1570 earthquake and tsunami

The earthquake of April 8, 1570, has an offshore origin in the epicentral region of Concepción with a magnitude approximately of M $\sim$ 8 - 8.5, causing a destructive tsunami (Lomnitz, 1970). By this time, as a result of an ongoing Mapuche communities uprising in the coastal towns of Cañete (Lebu), Arauco and the inland city of Angol, there are no historical records of tsunami in the area, although it is supposed these cities have been in the destruction radius of the earthquake and tsunami (Stewart**, 2019). Likewise, evidence of uplift in paleotsunami records in Tirúa suggest possible deposits from 1570 and 1575 events, however historical records suggests it can be more likely deposited by the 1575 event (Ely et al., 2014).

About the size earthquake it is hard to define from the available historical and geological observations, but what can be said it is that there is no meaningful damages in south Valdivia and north Santiago (Stewart**, 2019) and according to Soloviev, S.L., and Ch.N. Go (1975) the limits of the event are between 36.00°S and 38.00°S. It is presumed that the earthquake was not quite as large as May 22, 1960, or February 20, 1835, however, the effects of the shock were comparable to those of the 1835 earthquake (Lomnitz, 1970).

In addition, according to Lockridge (1985) the tsunami had a runup of 4 meters, a magnitude of 2.0 and intensity of 3.0 leaving the city submerged. The tsunami reports are limited to the Bay of Concepción and is described as an initial wave which flooded part of the town and returned several times (Lomnitz, 1970).

Some historical records mention a tsunamigenic earthquake occurred on October 28, 1562, but descriptions of 1570 and 1562 events are very similar. Therefore, it is possible that in reality only one catastrophic tsunami occurred in 1570

(Lomnitz, 1970; Soloviev et al., 1975). In this way, Lockridge suggest an earthquake magnitude of 8.0, tsunami magnitude of 4.0 and intensity of 3.5 besides runup of 16 meters.

Information about vertical deformation is not available; given the antiquity of this event, it is the least known due to the small amount of available data.

2.3.2 1657 earthquake and tsunami

The earthquake of March 15, 1657, similarly to the 1570 event, has an offshore origin in the epicentral region of Concepción (36.830°S, 73.030°W, according to NOAA), with an estimated magnitude of M $\sim$ 8 and a major tsunami (Lomnitz, 1970; Lockridge, 1985); Soloviev, et al. (1975) proposes the earthquake limits between 36°S and 39°S latitudes. Udías et al. (2012) suggest that the area of the earthquake had a very similar extent to that of the 1835 Darwin earthquake.

The tsunami is described with, at least, three large waves destroying everything that the earthquake left standing, inundation reached the center of the main square and lower sections of the town in old Concepción (Berninghausen, 1962; Soloviev, et al., 1975). According to Lockridge (1985) the tsunami magnitude is 3.0 and intensity 2.5, runup of 8 meters; further Valparaíso (33.08°S, 71.67°W) reports the tsunami. Its size was comparable to that of 1570 and of 1835, but the earthquake itself seems to have been slightly less severe (Lomnitz, 1970).

2.3.3 1751 earthquake and tsunami

Lomnitz (1970; 2004) provides a survey of historical earthquakes in Chile and describes the event of 25 May 1751 with a magnitude M $\sim$ 8.5 and an earthquake that destroyed the city of Concepcion, after which it was rebuilt at its present location with less exposure to tsunami damage. According to the author and references therein, the tsunami was larger than in 1657 and in 1730, propagating around the Pacific Ocean, including Callao, Peru (12.0°S), Juan Fernandez Islands, Chile (33.6°S) and Japan. Udias et al. (2012) used contemporary documents in the "Archivo General de las Indias" (AGI), to study in detail the 1647, 1657, 1730 and 1751 earthquakes. The authors called the 1751 earthquake as the second-largest after the 1730 earthquake in this period (17th and 18th centuries), suggesting that this event is very similar to the 2010 earthquake in terms of geometrical

features such as size and extent, and also because of the effects of the tsunami. The 1751 earthquake affected a region up to 100 km south of the end of the region affected by the 2010 earthquake. Earthquake damages extended from Santiago and Valparaiso in the north ($\sim 33°$S), and to Valdivia in the south (39.8°S).

In terms of vertical deformation, observations indicate a co-seismic uplift of 7 m at the bottom of Concepcion Bay (Soloviev and Go, 1975), categorical data of subsidence in Chillan (36.6°S), and uplift in Quiriquina (36.6°S) and Santa Maria Island (37.0°S) (Lomnitz, 2004; Quezada et al. 2012). The geographic locations of the observations are shown in Fig. 1.1.1. The uplift processes resulting from the earthquake were also detected through paleoseismological evidence at Tirua (38.2°S) and Quidico (38.3°S), assuming a rupture length > 600 km (Ely et al. 2014; Dura et al. 2015; Hong et al. 2017). The arrival of the tsunami wave was inferred from Stewart (2019) that presented tables with tsunami damages and water depth for historical tsunamis in the city of Penco (Chile), and from Lomnitz (1970; 2004) for Juan Fernandez Island (Chile) and in the coast of Ojika, Monou, Motoyoshi, and Kesen counties in Japan (Tsuji, 2013). Those sites (Penco, Juan Fernandez Island and Japan) were selected to validate the numerical modelling of the tsunami propagation.

2.3.4 1835 earthquake and tsunami

The extension of the 1835 earthquake is estimated approximately from 35.0° to 38.5°S (Metois et al., 2012; Quezada et al., 2012; Ruiz y Madariaga, 2018) Observations near Concepcion bay indicate unusually high values of deformation for an earthquake that has been prescribed with a length of about 300 km. Deformation values between 1 and 3 m are concentrated between 36.0° and 37°S (Caldcleugh, 1836; FitzRoy, 1839; Darwin, 1860; Pizarro, 1991; Lomnitz, 2004; Quezada et al. 2012). Several damages caused by the earthquake were perceived from Coquimbo to Castro (north to south direction) and from Mendoza to Juan Fernandez Island (east to west direction), tsunami effects were perceived from Valparaiso to Castro (Fitz-Roy, 1839; D'Urville, 1942; Soloviev and Go, 1975; Stewart, 2019), and the authors recorded waves from 3 to 12 meters approximately in the central zone (Penco Bay, Talcahuano, Boca Chica, Coelemu, Constitucion).

2.3.5 2010 earthquake and tsunami

The 2010 megathrust event occurred in the South Central segment in 2010. As one of the largest and most recent events in the world, this earthquake has been extensively studied, and there are abundant data and measurements to compare. It is assumed to be a Mw 8.8 megathrust earthquake, with about a ∼500 km rupture zone (Lay et al. 2010; Lorito et al. 2011; Pollitz et al. 2011; Vigny et al. 2011; Moreno et al. 2012; Ruiz & Madariaga, 2018). Uplift observation data are also available from Farias et al. (2010); Quezada et al. (2012) and Ely et al. (2014).

Chapter 3

Results

3.1 1570 and 1657 earthquakes and tsunamis

Despite efforts to characterize the earthquakes and tsunamis of 1570 and 1657, it was not possible to do so due to the lack of information. While we were able to gather some data to establish the logic tree parameters for each event, the absence of numerical and categorical vertical deformation observations to apply as constraints, resulted in the generation of thousands of models, indicating consistently homogeneous results. Therefore, all parameters were equally likely, and the model failed to converge.

3.2 1751 earthquake and tsunami

After evaluating 25200 candidate models, we identified 19 slip distribution models that were most likely to characterize the 1751 event. As no numerical data representing the tsunami wave height are available, no such constraint was performed, but the tsunami propagation was modeled from the final deformation model obtained for the event and compared with the available categorical data. The predicted deformation field succeeds in reproducing categorical observations. For numerical data, the model reproduces the observation with a tolerance of 3.5 m lower than the true value. The predicted deformation field also reproduces the propagation of the tsunami for both the Chilean and Japanese coasts, arriving at the latter after approximately 22 hours and reaching tsunami heights of 60 cm without considering tidal effects (Fig. 3.2.1).

The slip distribution model for the 1751 earthquake shows two main slip patches between 36.0° and 38.0° S (Fig. 3.2.1), positioned in an area of slab at depths about 30 to 40 km. A peak slip of ∼26 m over the Concepcion area is located in the biggest slip patch (within the Talcahuano and Penco Bay), and a second minor slip patch approximately between Cauquenes and Parral (36.0° - 36.5°S). Unlike 1835, and 2010, the rupture boundary to the south of the 1751 earthquake overlaps with the 1960 earthquake rupture in the Valdivia segment (Carvajal et al. 2017)

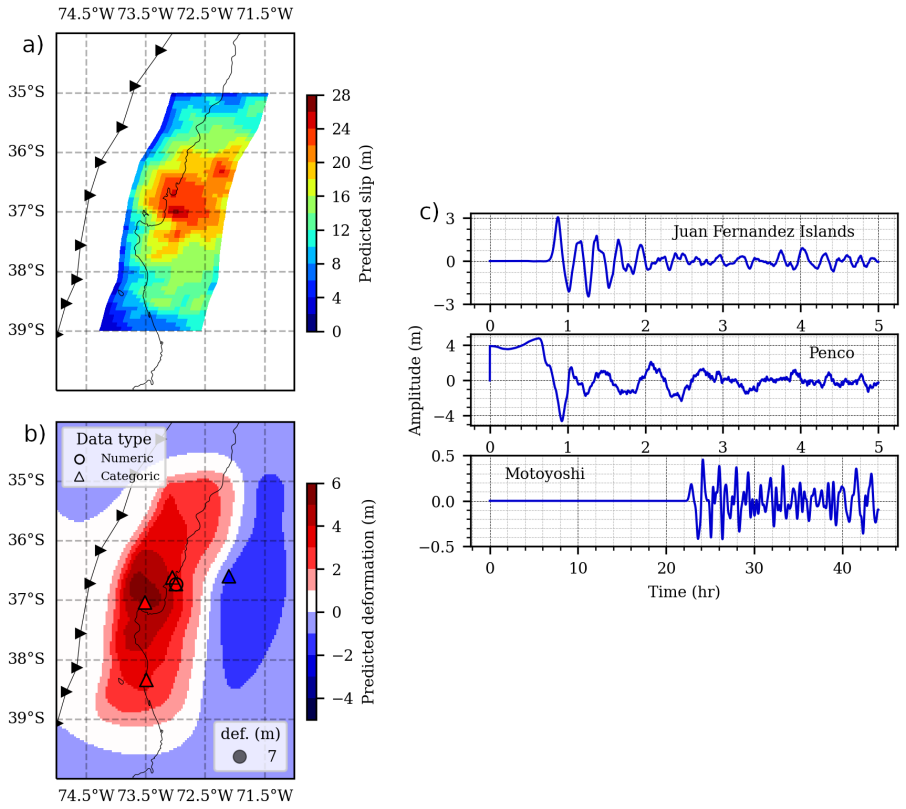

Figure 3.2.1: Figure a) Final estimation of heterogeneous slip distribution model for 1751 earthquake. Figure b) Vertical deformation field for 1751 earthquake. Deformation data with both categorical (triangle) or numerical (circle) observations is also shown. Red markers indicate uplift, blue markers indicate subsidence. Figure c) Wave amplitude from predicted tide gauges. Virtual tide gauge areas correspond to Juan Fernandez Islands (Chile), Penco, Concepcion Bay (Chile) and Coast of Motoyoshi in Japan from 1751 tsunami propagation.

3.3 1835 earthquake and tsunami

A total of 14400 random slip distribution models were generated for the 1835 earthquake, but only 10 models satisfied the deformation constraint. Since the observed tsunami height values by different authors exceeded 4 meters (Fitz Roy, 1839; D'Urville, 1842; Soloviev and Go, 1975) and deformation models did not satisfy the tsunami height observations, results were obtained from the final deformation model and compared maximum wave height predicted with numerical and categorical data.

For the 1835 earthquake, results suggests a rupture extent of approximately 330 km between 35.0° and 38.0° S. This model shows a main slip patch with a peak slip of ∼10 m at depths of about 20 km, located in the northern part of the rupture and mainly offshore. In an inter-event comparison, this earthquake presents much lower slip values, but deformation values are in agreement with the uplift observations collected. However, the deformation field did not reproduce subsidence observations. Virtual tide gauges located in central Chile show tsunami maximum wave heights of approximately 2 m (Fig. 3.3.1). We believe that the 1835 slip distribution model underestimates the parameters of tsunami wave height and rupture extent, possibly due to the low spatial resolution of data, particularly at the segment limits.

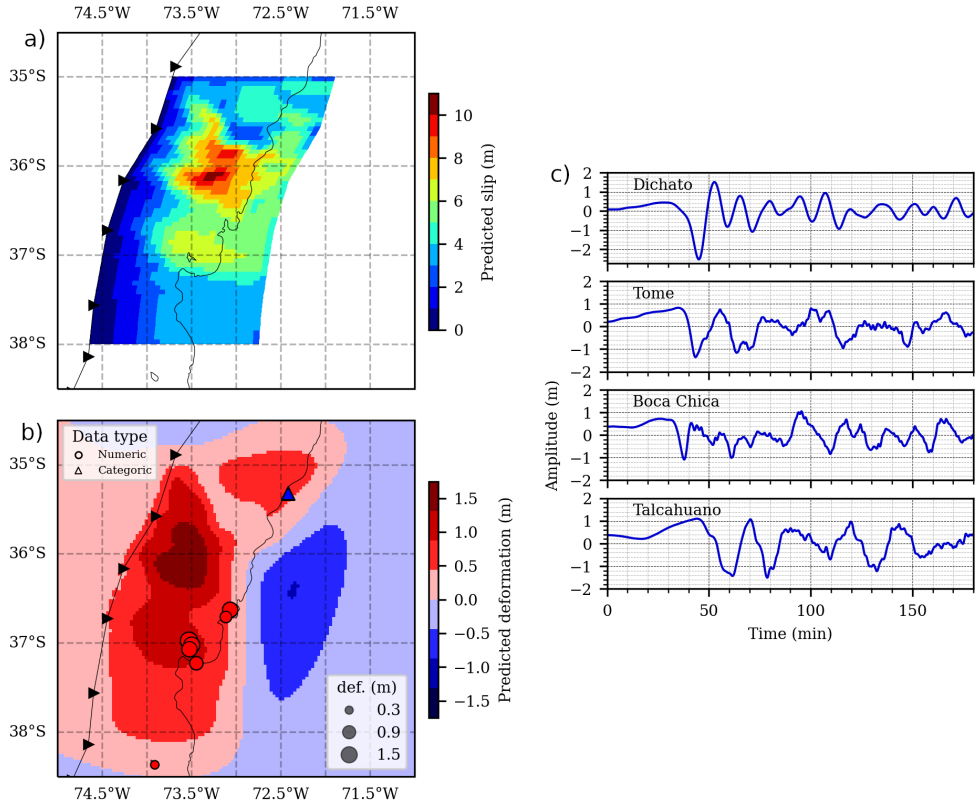

Figure 3.3.1: Figure a) Final estimation of heterogeneous slip distribution model for 1835 earthquake. Figure b) Vertical deformation field for 1835 earthquake. Deformation data with both categorical (triangle) or numerical (circle) observations is also shown. Red markers indicate uplift, blue markers indicate subsidence. Figure c) Wave amplitude from predicted tide gauges. Virtual tide gauge areas correspond to Dichato, Tome, Boca Chica, Talcahuano, respectively.

3.4 2010 earthquake and tsunami

We obtained a total of 8640 slip distribution models for the 2010 earthquake. However, only 10 of these models were found to be possible after applying deformation and tsunami constraints to accurately characterize the event.

The 2010 earthquake results shows a slip distribution model with a rupture zone that extends from 34.0° to 37.5° S, with the largest slip patches located in the northern portion of the rupture zone (34° - 35° S). Peak slip reaches approximately 16 m at depths about 15 to 20 km. A minor slip patch to the south reached a depth of approximately 10 m. The predicted deformation field also succeeds in reproducing deformation observations (Fig. 3.4.1). We also found that predicted

field deformation for tsunami propagation reproduces arrival times at SHOA tide gauges (see also Fig. 3.4.1).

Our findings are consistent with previous slip models obtained through inversions of seismic and deformation data, such as the one presented by Moreno et al. (2012), where the main slip patch is located in the northern portion of the segment with a slip amount of up to 16 m. Their model also includes south patches between 36° and 37°S with slip exceeding 10 m.

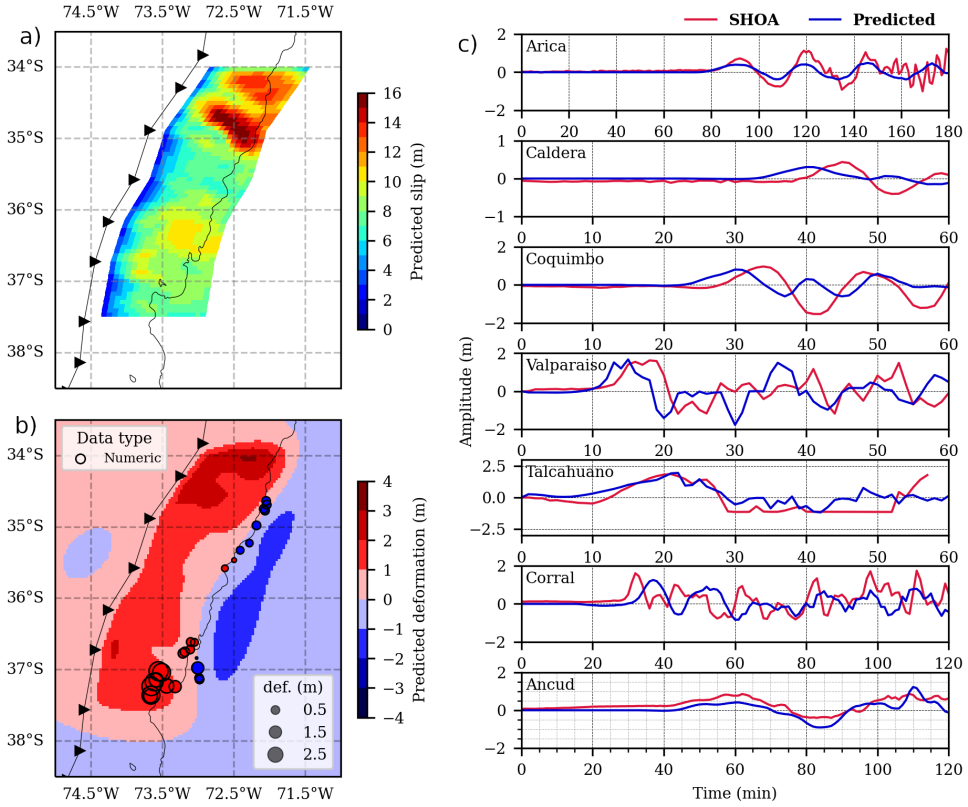

Figure 3.4.1: Figure a) Final estimation of heterogeneous slip distribution model for 2010 earthquake. Figure b) Vertical deformation field for 2010 earthquake. Deformation data numerical (circle) observations are also shown. Red markers indicate uplift, blue markers indicate subsidence. Figure c) Wave amplitude from predicted (blue lines) and SHOA (red lines) tide gauges.

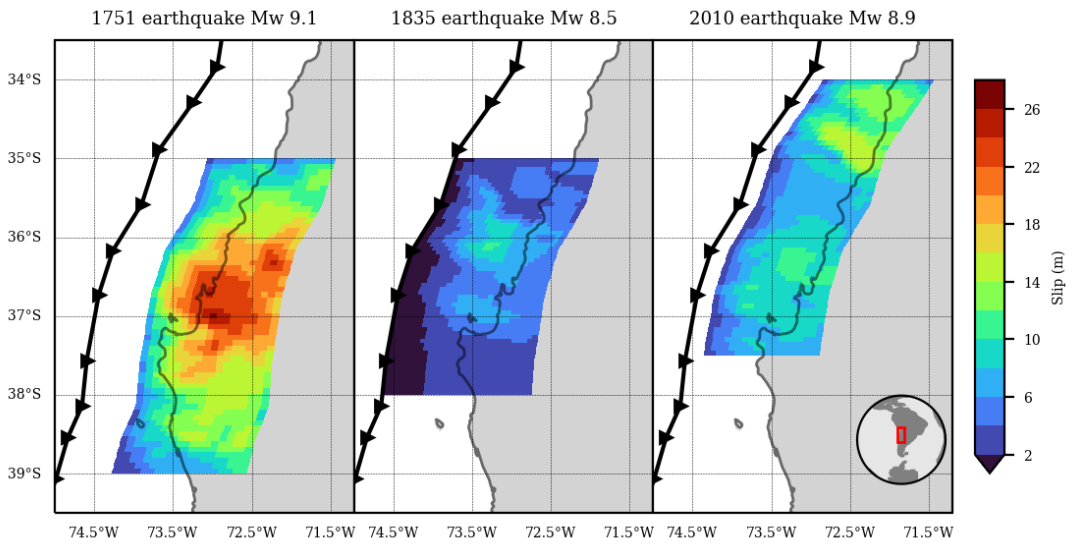

Figure 3.4.2: Final heterogeneous slip distribution models after applying Gaussian filtering and PDF maximization for each set of candidate fault models

Chapter 4

Discussion

We analyze slip distribution models to identify the portions of the segment that released the most energy. Because frictional properties vary in both directions, depth domains add complexity in pattern recognition (Lay et al. 2012). The spatio-temporal evolution of asperities gives insights into the rupture dynamics and recurrence intervals in a megathrust segment. Thus, understanding the slip sequence and depth of previous earthquakes, particularly the overlapping rupture areas, can provide insights into the future behavior of the segment. As was done by Carvajal et al. (2017) on the 1906 and 2010 earthquakes, which succeeded the 1730 and 1751 earthquakes, respectively, they infer a similar slip sequence in the intersegment zone where the rupture areas of the earlier earthquakes likely overlapped. These findings suggest that studying the slip depth and history of earthquakes can provide valuable information for seismic hazard assessments and disaster mitigation measures.

Our results suggest that the slip distribution model of the 1751 earthquake successfully reproduces the vertical deformation observations of Soloviev and Go (1975), Quezada et al. (2012), Ely et al. (2014), and Dura et al. (2017) regarding uplift or subsidence behavior (Fig. 3.2.1). Additionally, the predicted deformation field generated by the model aligns with the observed tsunami propagation presented in Tsuji (2013) and Soloviev and Go (1975), which reports that tsunami waves reached the coast of Japan. Despite having only one numerical deformation observation for the 1751 earthquake (around 7 m uplift in the bottom of Concepcion Bay, according to Soloviev and Go, 1975), the unusual amount

of deformation allowed for a more accurate selection of models that complied with the observation. To account for the uncertainty of observation, a generous tolerance of 3.5 m was set to generate a range of acceptable values. Nonetheless, it is important to note that the acceptable range of values may vary in the case of ancient earthquakes, showing larger uncertainties due to the limitations of recording methods at the time. Therefore, we consider that the tolerance used in this step is an accurate value.

The arrival of the signal from the 1751 tsunami modeling occurs after approximately 22 hours, which corresponds to a realistic period for transatlantic tsunami propagation. Nevertheless, we note that the model tends to underestimate the maximum wave heights (Fig. 4). The model suggests a magnitude Mw $\sim$ 9.1, which is in agreement with the estimate made by other authors (Udias et al. 2012; Carvajal et al. 2017; Ruiz and Madariaga, 2018) who also propose an M $\sim$ 9 and even higher, in contrast with the magnitude Ms $\sim$ 8.5 suggested by previous works for this event (Lomnitz, 2004). Because the depths of the slip distribution are between in 30 to 40 km, we consider this earthquake as shallow or typical slip inferred, in agreement with the discussion made by Carvajal et al. (2017). The southern limit of slip in the 1751 earthquake of approximately 39° in our model (Fig. 3.2.1) also reproduces the suggestion from paleoseismological studies that 1751 had a larger southern extension than that of the 2010 earthquake, which has been shown to extend to approximately 38.5° (Melnick et al. 2012; Ely et al. 2014).

This event is very different from 1835 and 2010, which are both shallower events with slips close to the trench. In the case of 1751, the results indicate that it is the deepest event of the three with the highest amount of slip, having values above 20 m. After this event, successors also show patches of slips between 36° and 37°S, but their asperities are close to the trench. This latitudinal band repeats the slip pattern, along strike, in all three models. To better understand the seismic cycle, it is necessary to recognize the places where the slip patches are repeated, as well as the places that do not present significant slips and the behavior of these zones in the coupling models.

We consider that the 1835 earthquake initiated the seismic gap closed by the 2010 event, but we do not interpret it as a predecessor earthquake. We anticipate that a predecessor earthquake will not only precede the current one in time, but

will also share similar characteristics with the subsequent event, such as rupture length, position of asperities, depth, and northern and southern limits.

The 1835 earthquake does not meet these conditions, as it has a smaller rupture length and a smaller and different location of the main slip patch. The 2010 earthquake repeats the slip pattern between 36° and 37°S. Although that is not its highest magnitude patch, it is still one of the areas with the greatest slip within the entire rupture length of the segment.

In the same way, for the 1751 earthquake, although it is a similar size, our results show different positions, patches and magnitudes of slip. These results indicate that none of these events are predecessors of the others, but they may have contributed to the occurrence of the successors.

In the 1751, 1835 and 2010 earthquakes the rupture crossed the Arauco peninsula, unlike the 1960 and 1953 earthquakes, where this peninsula played a role as a seismic barrier, slowing the northward propagation of these events (Melnick et al. 2009; Quezada et al. 2012). We suggest that the Arauco peninsula does not act as a persistent barrier but as a possible frequent barrier according to the type of barriers proposed by Philibosian et al. (2020). It represents a barrier that is occasionally traversed, but often stops ruptures.

With additional paleoseismic data, analysis of the characteristics of pre-historic earthquakes using this methodology could show more similarities or variations in depth, asperities, rupture extension, and magnitude. Such results may reveal recurrence intervals in the seismic cycle. However, to fully understand the seismic cycle, it must be viewed as a process composed not only of megathrust earthquake ruptures, but of the other dynamics that contribute to energy accumulation.

Chapter 5

Conclusion

This work aims to reconstruct historical earthquakes, specifically the 1570, 1657, 1751, 1835 and 2010 megathrust earthquakes that overlapped in the South Central segment. These events had significant implications in both geophysical and social aspects. By understanding the geophysical processes, including the spatio-temporal evolution of the seismic cycle, we can enhance the resilience of communities exposed to this type of natural hazard. Therefore, through this work, we can identify rupture patterns and areas that did not experience energy release as a result of the earthquake.

The methodology applied here is well-suited for numerical testing and produces model results that comply with both numerical and categorical data observations. However, in cases where data availability is limited, it tends to underestimate results. The accuracy of a slip distribution model depends on the quality and quantity of the data used to constrain the model, as well as the complexity of the geological and seismological conditions of the studied area. Nevertheless, the methodology can provide valuable information about earthquakes themselves, as well as similarities or differences with subsequent events.

The slip distribution results of the 2010 earthquake are consistent with prior studies, reproducing the location and observations of the primary slip patches. However, our model underestimates the southern extent of the rupture, which has been inferred to be at least 38.5° and differs from the Mw 8.8 magnitude suggested by Vigny et al. (2011), Moreno et al. (2012), and Quezada et al. (2012). After conducting a frequency analysis, we found that the most frequently occurring

magnitude was Mw 8.9. Our results are considered a realistic approximation that could be improved by including a broader range of parameters in the logic tree branches.

In contrast, the slip distribution model for the 1751 earthquake showed less shallow but greater slip, with the main patch located at a depth of 30-40 km and reaching magnitudes of approximately 26 m. This event also had the greatest extension to the south of the segment. Our model successfully reproduced categorical data, which was the primary available data in this case. Managing the accuracy of numerical data is challenging because observations are limited. Despite this, our model aligns with the data trends.

Regarding the 1835 earthquake, our slip distribution model was able to reproduce the tsunami propagation and deformation data, though the deformation field did not indicate subsidence in Constitucion, as categorical data suggested. We consider this event to be a special case where the southern rupture extension may have been greater than previously proposed. Future experiments may benefit from a wider range of values for southern limits. Like the 1751 earthquake, both events lacked rupture extent in the northern portion of the segment, which was eventually broken by the 2010 Maule earthquake. Our findings suggest that the northern part of the segment had been accumulating energy for at least 300 years. Nonetheless, it is crucial to have sufficient data to reproduce the slip distribution models of precursor earthquakes, such as those in 1570 and 1657.

The primary constraint we encountered was the limited availability of data on historical earthquakes in the South Central segment, particularly for the years 1570 and 1657. Available resources provide valuable information on the 1657 earthquake (Stewart, 2021). However, they were not enough to apply the logic tree method. Despite generating random sources, we were unable to obtain meaningful results due to insufficient deformation data, which restricted our ability to refine the computed fields. To improve this work, it is necessary to increase the amount of historical events and acquire more data to refine the models. Additionally, to gain a better understanding of the seismic cycle, we recommend incorporating other deformation and stress loading processes that also contribute to the cycle.

Bibliography

[1] Beck, S., S. Barrientos, E. Kausel, and M. Reyes (1998). Source characteristics of historic earthquakes along the central Chile subduction zone, Journal of South American Earth Sciences 11, 115-129.

[2] Bilek, S. L., & Lay, T. (2018). Subduction zone megathrust earthquakes. Geosphere, 14(4), 1468-1500.

[3] Carvajal M., Cisternas M., Catalán P. (2017) Source of the 1730 Chilean earthquake from historical records: implications for the future tsunami hazard on the coast of metropolitan Chile. J Geophys Res Solid Earth 122(5):3648–3660

[4] Caldcleugh, A. (1836). III. An account of the great earthquake experienced in Chile on the 20th of February, 1835; with a map. Philosophical Transactions of the Royal Society of London, (126), 21-26.

[5] Cifuentes-Lobos, R., Calisto, I., MacInnes, B., Moreno, M., Quezada, J., San Martín, J., Fernandez-Palma, M., & Saavedra, C. (2023). A stochastic approach to the characterization of the seismic sources: a potential method for the assessment of sources of historical and paleo tsunami. Stochastic Environmental Research and Risk Assessment, 1-13.

[6] Darwin, C. (1860). A naturalist's voyage round the world. Journal of researches.

[7] Delouis, B., Nocquet, J. M., & Vallée, M. (2010). Slip distribution of the February 27, 2010 Mw= 8.8 Maule earthquake, central Chile, from static and high-rate GPS, InSAR, and broadband teleseismic data. Geophysical Research Letters, 37(17).

[8] Dura, T., Cisternas, M., Horton, B. P., Ely, L. L., Nelson, A. R., Wesson, R.

L., & Pilarczyk, J. E. (2015). Coastal evidence for Holocene subduction-zone earthquakes and tsunamis in central Chile. Quaternary Science Reviews, 113, 93-111.

[9] Dura, T., Horton, B. P., Cisternas, M, Ely, L. L., Hong, I., Nelson, A. R., Wesson, R. L., Pilarczyk, J. E., Parnell, A. C., Nikitina, D. (2017). Subduction zone slip variability during the last millennium, south-central Chile. Quaternary Science Reviews, 175, 112-137.

[10] D'urville, M. D. (1842). Voyage au Pôle sud et dans l'Océanie sur les corvettes l'Astrolabe et la Zelée.

[11] Ely, L. L., Cisternas, M., Wesson, R. L., & Dura, T. (2014). Five centuries of tsunamis and land-level changes in the overlapping rupture area of the 1960 and 2010 Chilean earthquakes. Geology, 42(11), 995-998.

[12] Farias, M., Comte, D., Roecker, S., Carrizo, D., Pardo, M. (2011). Crustal extensional faulting triggered by the 2010 Chilean earthquake: the Pichilemu seismic sequence. Tectonics 30 (6)

[13] FitzRoy, R. (1839). Narrative of the Surveying Voyages of His Majesty's Ships Adventure and Beagle, Between the Years 1826 and 1836, Describing Their Examination of the Southern Shores of South America, and the Beagle's Circumnavigation of the Globe... (Vol. 2). Henry Colburn, Great Marlborough Street.

[14] Hong, I., Dura, T., Ely, L. L., Horton, B. P., Nelson, A. R., Cisternas, M., et al. (2017). A 600-year-long stratigraphic record of tsunamis in south-central Chile. The Holocene, 27(1), 39-51.

[15] Lay, T., Ammon, C.J., Kanamori, H., Koper, K.D., Sufri, O., Hutko, A.R. (2010). Teleseismic inversion for rupture process of the 27 February 2010 Chile (Mw 8.8) earthquake. Geophys. Res. Lett. 37 (13).

[16] Lay, T., Kanamori, H., Ammon, C.J., Koper, K.D., Hutko, A.R., Ye, L., Yue, H., Rushing, T.M. (2012). Depth-varying rupture properties of subduction zone megathrust faults. J. Geophys. Res. 117 https://doi.org/10.1029/2011JB009133. Article B04311.

[17] Lomnitz, C. (1970). Major earthquakes and tsunamis in Chile during the period 1535 to 1955, Geologische Rundschau 59, 938-960.

[18] Lomnitz, C. (2004). Major earthquakes of Chile: a historical survey, 1535-1960. Seismological Research Letters, 75(3), 368-378.

[19] Lorito, S., Romano, F., Atzori, S., Tong, X., Avallone, A., McCloskey, J., Cocco, M., Boschi, E., Piatanesi, A. (2011). Limited overlap between the seismic gap and coseismic slip of the great 2010 Chile earthquake. Nat. Geosci. 4 (3), 173.

[20] Melnick, D., Bookhagen, B., Strecker, M.R., Echtler, H.P. (2009). Segmentation of megathrust rupture zones from fore-arc deformation patterns over hundreds to millions of years, Arauco peninsula, Chile. J. Geophys. Res. 114 https://doi.org/10.1029/2008JB005788.

[21] Moreno, M., Melnick, D., Rosenau, M., Baez, J., Klotz, J., Oncken, O., et al. (2012). Toward understanding tectonic control on the Mw 8.8 2010 Maule Chile earthquake. Earth and Planetary Science Letters, 321, 152-165.

[22] Métois, M., Socquet, A., & Vigny, C. (2012). Interseismic coupling, segmentation and mechanical behavior of the central Chile subduction zone. Journal of Geophysical Research: Solid Earth, 117(B3).

[23] Nishenko, S.P., 1991. Circum-Pacific seismic potential: 1989e1999. Pure Appl. Geophys. 135, 169e259. https://doi.org/10.1007/BF00880240.

[24] Okada Y (1985) Surface deformation due to shear and tensile faults in a half-space. Bull Seismol Soc Am 75(4):1135–1154

[25] Pizarro, J. 1991. Lebu: de la Leufumapu a su centenario 1540-1962. Editorial Ñielol: 398 p. Santiago.

[26] Philibosian, B., & Meltzner, A. J. (2020). Segmentation and supercycles: A catalog of earthquake rupture patterns from the Sumatran Sunda Megathrust and other well-studied faults worldwide. Quaternary Science Reviews, 241, 106390. https://doi.org/10.1016/j.quascirev.2020.106390

[27] Pollitz, F. F., et al. (2011), Coseismic slip distribution of the February 27, 2010 Mw 8.8 Maule, Chile earthquake, Geophys. Res. Lett., 38, L09309, https://doi:10.1029/2011GL047065.

[28] Quezada, J., Jaque, E., Fernández, A., & Vásquez, D. (2012). Cambios en el relieve generados como consecuencia del terremoto Mw= 8, 8 del 27 de febrero de 2010 en el centro-sur de Chile. Revista de Geografía Norte Grande, (53), 35-55.

[29] Ruiz S., Madariaga R. (2018) Historical and recent large megathrust earthquakes in Chile. Tectonophysics 733:37–56

[30] Soloviev, S. L., & Go, C. N. (1975). A catalogue of tsunamis on the eastern shore of the Pacific Ocean (1513–1968), translated by Canadian Institute for Scientific and Technical Information, National Research Council Ottawa.

[31] Stewart, D. M. (2019). Historical tsunamis in the Concepcion bay, as seen in the reconstructed flood levels from the colonial city of Concepcion (Penco), Chile (1570–1835). Revista de historia (Concepción) 26(2):97–127. https://doi.org/10.4067/S0717-88322019000200097

[32] Stewart, D. M. (2021). El terremoto de 1657 en Concepción, Chile. Un analogo colonial del terremoto en Maule 2010. Cuadernos de historia (Santiago), (55), 191-221.

[33] Tsuji, Y. (2013). Catalog of distant tsunamis reaching Japan from Chile and Peru. Rep. Tsunami Eng, 30, 61-68.

[34] Udias, A., Madariaga, R., Buforn, E., Muñoz, D., Ros, M., 2012. The large Chilean historical earthquakes of 1647, 1657, 1730, and 1751 from contemporary documents. Bull. Seismol. Soc. Am. 102, 1639–1653.

[35] Vigny, C., Socquet, A., Peyrat, S., Ruegg, J. C., Métois, M., Madariaga, R., et al. (2011). The 2010 M w 8.8 Maule megathrust earthquake of central Chile, monitored by GPS. Science, 332(6036), 1417-1421.

[36] Wang X (2009) User manual for comcot version 1.7 (first draft). Cornel University 65.